ACS APPLIED ENERGY MATERIALS
Cite This: ACS Appl. Energy Mater. 2019, 2, 3972−3978
Letter
www.acsaem.org

Lead Halide Ultraviolet-Harvesting Transparent Photovoltaics with an Efficiency Exceeding 1%

Dianyi Liu,[†,‡,∥] Chenchen Yang,[†,∥] Pei Chen,[†] Matthew Bates,[†] Songyang Han,[†] Per Askeland,[†] and Richard R. Lunt*[,†,§]

[†]Department of Chemical Engineering and Material Science, Michigan State University, East Lansing, Michigan 48824, United States

[‡]School of Engineering, Westlake University, 18 Shilongshan Road, Hangzhou 310024, China

[§]Department of Physics and Astronomy, Michigan State University, East Lansing, Michigan 48824, United States

Supporting Information

ABSTRACT: Transparent photovoltaic (TPV) devices have a number of unique advantages compared with opaque photovoltaic devices. However, balancing efficiency and transparency has been difficult. To date, few TPV devices with PCE over 1% have been demonstrated when the average visible transmission (AVT) is over 70%. Here, we report a series of lead halide based TPVs with both increased efficiency and transparency. The effects of lead halide layer thickness and composition were systematically studied. Subsequently, the efficiency, transparency, and stability of lead halide TPVs were evaluated. Results show that lead halide TPVs with ultraviolet (UV) wavelength-selective absorption can achieve efficiencies over 1% while the AVT is above 70%. This study provides a simple approach to prepare UV-harvesting TPVs with high efficiency and high visible transparency that are potentially viable as single-junction cells or as a component of multijunction transparent and opaque cells.

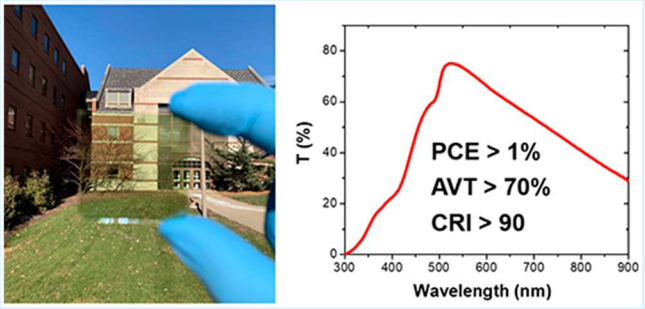

KEYWORDS: *lead halide, solar cells, solution-processing, transparent photovoltaic, ultraviolet*

Wavelength-selective transparent photovoltaics (TPVs) focus on converting invisible light to electric power while allowing the majority of visible light (VIS) to pass through. This new functionality provides great potential for deployment in nontraditional applications.[1,2] There are several primary parameters of interest in TPVs: power conversion efficiency (PCE), average visible transmission (AVT), and color rendering index (CRI).[1] AVT is actually just as important as PCE since it often defines the minimum threshold for deploying TPVs in new applications. In addition, the CRI is another important parameter for the adoptability of TPVs. Although the PCE of TPVs has been significantly improved to over 5% (with AVTs between 50%−55%) in just the past several years,[1] much work has been focusing on semitransparent PVs even though many of the emerging applications are only enabled at the highest AVTs above 70% (Figure S1).[1,3] Notably, the efficiencies of TPVs drop sharply when the AVT exceeds 60%, which highlights the challenge of improving the efficiency of TPVs with high transparency.

To improve the AVT and CRI of TPVs, decreasing the absorption of visible light is key. Here we focus on approaching the highest level of AVT. A few reports have looked to selectively utilize the ultraviolet (UV) light or near-infrared (NIR) light absorption materials to produce the highest transparency devices.[4−8] A series of organic salts with NIR-harvesting properties and efficiency up to 0.9% with AVT of 60.4% were demonstrated by our group.[4] Geiger and colleagues similarly reported organic based NIR absorbing TPVs with PCEs between 0.9% and 2.2% and AVT values (450−670 nm) of 62−66%.[6] Loo et al. reported a UV-harvesting organic TPV which achieved an AVT of 60% with a PCE of 1.5%.[7] In our previous work, we developed a halide perovskite based UV-selective photovoltaic device with a PCE of 0.52% and an AVT up to 73% by exploiting the sharp wavelength cutoff enabled by tuning the perovskite bandgap right around the UV−vis cutoff.[8] However, these previous efforts to develop highly transparent TPVs have shown that it is difficult to improve the TPV efficiency over 1% while the AVT simultaneously exceeds 70% due to the complex film fabrication process, optical losses, and the large photovoltage loss in devices, even though the theoretical limits for UV- and UV−NIR-harvesting TPVs are above 7% and 21%, respectively. Perovskite solar cells with thin and segmented absorbing layers are viable candidates for semitransparent PVs and TPVs

Received: February 8, 2019
Accepted: May 14, 2019
Published: May 14, 2019

DOI: 10.1021/acsaem.9b00270
ACS Appl. Energy Mater. 2019, 2, 3972−3978

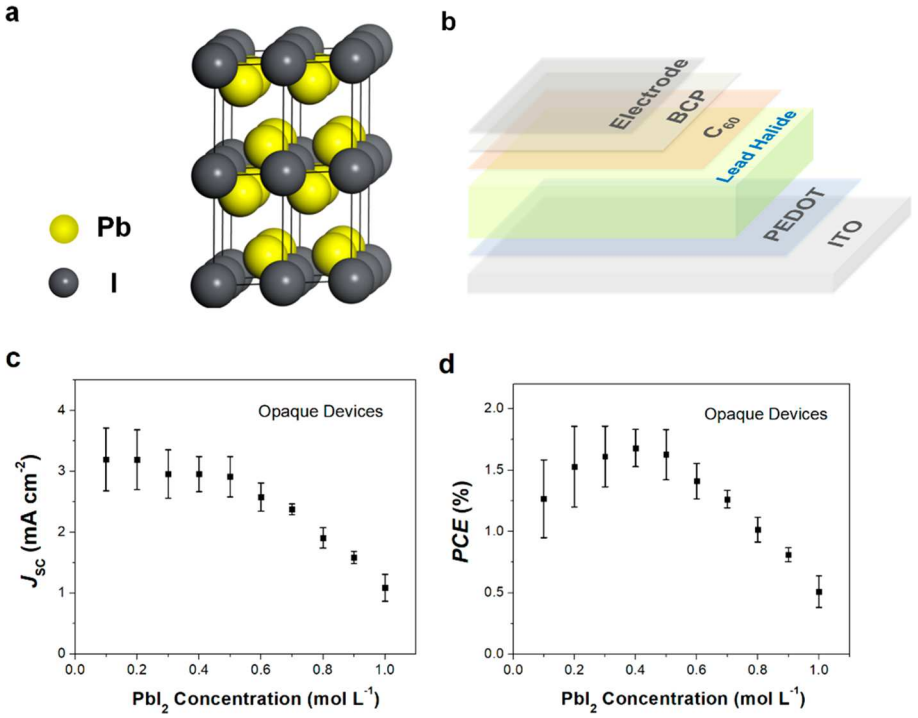

Figure 1. Structure and solar cell parameters for PbI_2: (a) PbI_2 crystal structure, (b) architecture of lead halide solar cells, (c) short-circuit current, and (d) power conversion efficiency of opaque PbI_2 solar cells prepared by PbI_2 precursor solutions with various concentrations. The error bars show the standard deviation for opaque devices where two batches of devices (7−8 devices for each condition) are used for the standard deviation calculation.

(Figure S1). However, due to the strong visible absorption of many perovskite solar cell materials, the ability to achieve good performance has been constrained at the highest levels of transparency.[9]

There are several types of metal halide semiconductors that exist including bulk semiconductors and metal halide nanoclusters.[10−12] The latter have been introduced to luminescent solar concentrators (LSCs) and light-emitting diodes (LEDs) as a phosphorescent material, while the former have emerged as a byproduct from research on metal halide perovskite solar cells.[11−13] Several metal halide semiconductors have already been used as the light absorber in opaque solar cells, indicating the potential of metal halide materials in photovoltaic applications.[14−16] Recently, an InI based solar cell (bandgap of 2.0 eV) was reported by the Mitzi group.[15] Although the device efficiency is only 0.4%, the study still suggests that InI is a viable photovoltaic material. Bismuth iodide (bandgap of 1.72 eV) has also been used in solar cells as the light harvest material, and the efficiency of the photovoltaic devices has been shown up to 1.2%.[16] However, since the bandgaps are in the visible range, these two metal halide materials are less suitable as a wavelength-selective light absorber in TPVs. Stemming from research on lead halide perovskite solar cells, PbI_2 (a common perovskite precursor) was found to function as a photovoltaic material.[10] While the bandgap of PbI_2 (2.4 eV) makes it less suitable for single-junction opaque cells (Figure S2),[10] it has the potential for selectively harvesting UV light for TPVs, particularly if the bandgap can be increased closer to 2.7−2.8 eV. Earlier this year, Chu et al. demonstrated PbI_2 as the light absorber for the TPVs with an efficiency up to 0.75%, with a corresponding AVT of 49%, but with a low CRI of 77.[17]

In this work, we demonstrate lead halide based TPVs with an efficiency over 1%. The thickness and processing of the PbI_2 active layer were first optimized. Chlorine (Cl) and bromine (Br) doping was also systematically investigated to understand the ability to modulate the bandgap. While it is anticipated that such modulation would be possible on the basis of work from the perovskite field, we demonstrate that such an approach will work with bulk metal halides (nonperovskite structures) and show the impact on physical and optoelectronic properties. We find that although the optical properties vary smoothly with doping there is a sharp drop in electronic properties with Br and Cl doping past 10−30%. On the basis of this optimization, the resulting lead halide TPVs show device PCEs up to 1.22% with an AVT of 70.7%. Initial device stability was studied to further understand the impact of compositional doping, where bromine doping is found to increase lifetime. This work demonstrates that simple lead halide semiconductors do indeed have good potential as light-harvesting materials for TPVs, and can be used to fabricate TPVs with high efficiency at the highest transparencies. The low cost and simple processing technique of lead halides provide a potential approach for TPVs in a variety of applications.

RESULTS

PbI_2 is a well-known precursor material for lead halide perovskite films that has a hexagonal crystal structure (Figure 1a).[18] PbI_2 films can be easily deposited on substrates by spin-coating or thermal evaporation as it is often a precursor layer for perovskite films,[18−20] and the film thickness can be controlled by changing the concentration of precursor solutions or spin-coating speed.[17,18] The influence of PbI_2 film thickness on device performance is first investigated in opaque device structures. PbI_2 precursor solutions are prepared

DOI: 10.1021/acsaem.9b00270
ACS Appl. Energy Mater. 2019, 2, 3972−3978

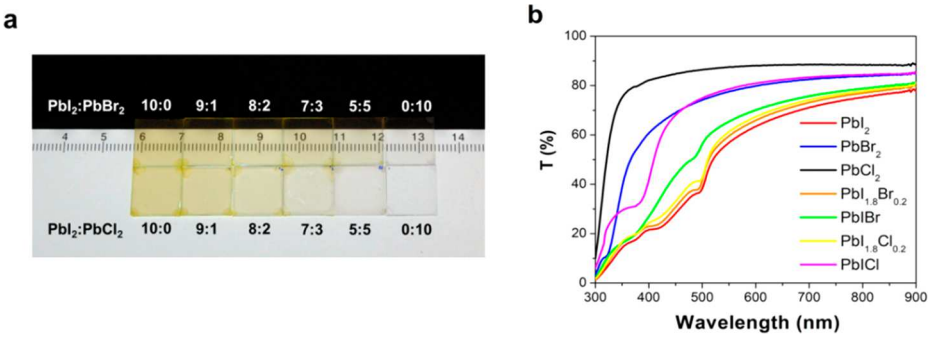

Figure 2. Optical characterization of lead halide films. (a) Photographs and (b) transmission spectra of lead halide films with various bromine or chlorine doping ratios (the concentration of lead is 0.3 M).

with concentrations ranging from 1 to 0.1 M. The thickness of the PbI_2 film increases from 9 ± 1 to 93 ± 2 nm as the solution concentration increases from 0.1 to 1.0 M (Figure S3). Since the processing atmosphere can significantly affect the morphology of PbI_2 films,[17,21] we adopt the vacuum-assistant method to prepare highly reproducible and smooth PbI_2 films in this study.[22] As seen in Figure S4, scanning electron microscopy (SEM) images show that PbI_2 films are uniform and smooth with few pinholes. A similar device architecture from our previous perovskite solar cell research is utilized in this work (Figure 1b),[22] where a thin poly(3,4-ethylenedioxythiophene) polystyrenesulfonate (PEDOT) layer acts as the hole extraction layer and a 20 nm fullerene layer is deposited on the PbI_2 to act as electron extraction layer. A thin 2,9-dimethyl-4,7-diphenyl-1,10-phenanthroline (BCP) layer is deposited on the fullerene to make ohmic contact with an 80 nm Ag electrode that is thermally evaporated. For the transparent devices, the Ag electrode is replaced with 5 nm Ag/60 nm tris(8-hydroxy-quinolinato) aluminum (Alq_3) as the transparent electrode.

Photovoltaic parameters of opaque devices are summarized in Figure 1 and Figure S5. The device photocurrent density drops as the PbI_2 film thickness increases. We infer that charge recombination increases with the PbI_2 film thickness due to modest charge collection lengths (or depletion widths) <40 nm. The charge recombination also reduces the open-circuit voltage (V_{OC}) of the device where the V_{OC} of the thickest PbI_2 film is lower than 1.0 V (Figure S5b). In comparison, the V_{OC} of the devices with a film thickness around 30 nm is around 1.1 V, and the highest V_{OC} recorded is 1.17 V. With only a modest drop in the voltage at the largest thicknesses, it is unlikely that there are underlying carrier interface barriers at the electrodes or the depletion width is larger than 90 nm.[23] The average PCE then shows a maximum value of 1.68% at 0.4 M. This result is utilized as a guide for TPV fabrication. While we aim to exploit the sharp bandgap cutoff to more selectively harvest ultraviolet light, thicker PbI_2 films can still decrease the transparency of TPV device and color rendering due a bandgap less than 2.75 eV. Thus, the concentration of PbI_2 precursor solutions are constrained below 0.3 M resulting in a thickness of PbI_2 film less than 30 nm for TPV devices.

We further demonstrate that the absorption range of lead halide materials can be modified by doping with various halide elements, analogous to perovskite films despite the vastly different crystal structure (hexagonal versus perovskite) and a more complex doping mechanism.[8,24−26] This is advantageous because it can enable precise bandgap modification around the UV−vis cutoff that we have shown to be critical for the optimization of both PCE and AVT in our previous work for halide perovskites.[8] Figure 2a shows photographs of PbI_2 films with various bromine or chlorine doping ratios. As Br or Cl doping increases, the light-yellow color becomes clearer and lighter. Accordingly, the transparency of the films increases concomitantly (Figure 2b). Notably, the bandgap of the PbI_2 film changes only slightly (<0.05 eV) when the Br doping ratio is less than 50%. The same doping effect is observed with Cl doping when the Cl ratio is less than 30%. However, when the Cl doping ratio reaches 50%, the bandgap abruptly changes by 0.5 eV (Figure S6 and Table S1). The conductivity and mobility of both pure PbI_2 and doped films are also evaluated. Figure S7 shows that Br/Cl doping decreases film conductivity and carrier mobility. The results indicate that the doping cannot improve the carrier mobility as it does for lead halide perovskite films.[27] Therefore, a low Br/Cl doping level is needed to maintain good semiconductor performance of the PbI_2 films.

Similar to the morphology of a pure PbI_2 film, the doped lead halide films are also uniform and smooth (Figure S8). X-ray diffraction (XRD) patterns of Br doped lead halide films show that the diffraction intensities are enhanced with a molar doping ratio of 10−50% (Figure S9), which indicates that Br doping contributes to improved film crystallization. Diffraction peaks shift to higher 2θ angles with increasing Br content leading to a smaller lattice constant due to the smaller ionic radius compared to the pure PbI_2 lattice. In contrast, the diffraction intensity of the Cl doped films does not change and the diffraction peaks do not shift. The differing doping effects of Br and Cl indicate a more complex doping behavior of lead halide materials compared to perovskites, likely due to a lack of isostructural similarity among PbI_2, $PbBr_2$, and $PbCl_2$ (the crystal structures of PbI_2, $PbBr_2$, and $PbCl_2$ are hexagonal, polymeric, and orthorhombic, respectively).[28,29] Owing to the complex doping effect of the lead halide films, the device photovoltaic parameters including V_{OC} do not show the expected change, and the doping mechanism on lead halide semiconductors warrants further studies. However, the performance of the corresponding device shows a sharp reduction when the doping ratio increases above 10% for Cl doping and 30% for Br doping (Figure S10). The elementary doping ratio is confirmed by X-ray photoelectron spectroscopy (XPS) as tabulated in Table S2. Subsequent TPV doping optimization was then performed around a 10% doping limit for both Cl and Br doping.

Lead halide TPVs are prepared with bromine or chlorine doped PbI_2 precursor solutions (10%) with the various solution concentrations of 0.1, 0.2, and 0.3 M. Photographs

DOI: 10.1021/acsaem.9b00270
ACS Appl. Energy Mater. 2019, 2, 3972−3978

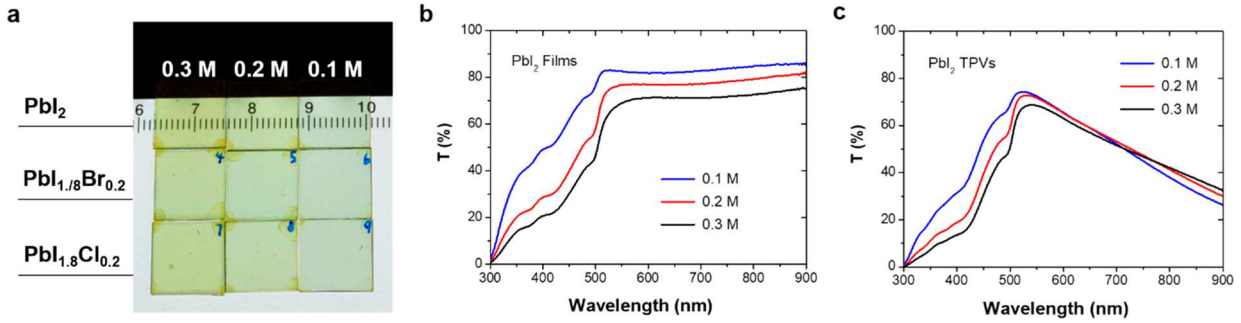

Figure 3. Optical characterization of lead halide TPV devices. (a) Photographs of the TPVs. Transmission spectra of (b) PbI_2 films and (c) TPVs prepared by PbI_2 precursor solutions with various concentrations.

Table 1. Summary of Photovoltaic and Transparency Parameters for Lead Halide TPVs[a]

device	[Pb] [M]	J_{SC} [mA cm^{-2}]	V_{OC} [V]	FF [%]	PCE [%]	AVT (%)	CRI
PbI_2	0.1	1.94 ± 0.14	0.998 ± 0.03	51.9 ± 1.7	1.00 ± 0.06	65.9	87.5
	0.2	2.02 ± 0.08	1.07 ± 0.02	55.0 ± 1.0	1.19 ± 0.06	69.2	89.3
	0.3	1.88 ± 0.05	1.02 ± 0.04	53.2 ± 2.3	1.02 ± 0.06	70.7	91.3
$PbI_{1.8}Br_{0.2}$	0.1	2.01 ± 0.06	1.02 ± 0.02	55.9 ± 1.6	1.15 ± 0.07	65.8	88.8
	0.2	2.00 ± 0.05	1.05 ± 0.02	55.1 ± 1.5	1.16 ± 0.05	69.1	90.2
	0.3	1.82 ± 0.04	0.966 ± 0.01	51.0 ± 3.6	0.929 ± 0.08	68.8	91.4
$PbI_{1.8}Cl_{0.2}$	0.1	1.92 ± 0.09	1.03 ± 0.01	54.7 ± 0.9	1.09 ± 0.06	64.0	88.7
	0.2	1.85 ± 0.09	1.07 ± 0.02	54.6 ± 1.5	1.08 ± 0.08	68.8	90.6
	0.3	1.72 ± 0.02	0.889 ± 0.04	55.2 ± 1.8	0.846 ± 0.03	70.5	92.1

[a]Two batches of devices (7−8 devices for each condition) are used for the standard deviation calculation.

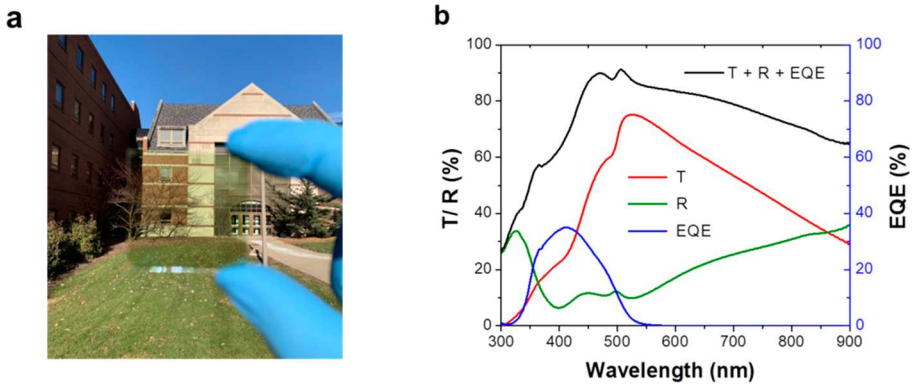

Figure 4. Characterization of lead halide TPV devices. (a) Photograph of fully assembled (unpatterned) device and (b) transmission (T), reflection (R), and external quantum efficiency (EQE) spectra of the $PbI_{1.8}Br_{0.2}$ TPV device.

of the fully assembled (unpatterned) TPV devices are shown in Figure 3a. Quantitative transparency parameters (AVT and CRI) for the TPVs are summarized in Table 1 including AVT and CRI. Figure 3b,c shows the transmission spectra of PbI_2 films and TPVs prepared from various concentrations of lead halide precursor solutions. Figure 3b shows that the transmission of 0.1 M PbI_2 film exceeds 80% from 510 to 900 nm. Accordingly, the 0.3 M PbI_2 film shows a peak transmission around 70%, and as a result, the AVT of TPVs decreases from 68.4% to 63.5%, respectively (Figure 3c). The AVT of devices increases as the thickness of the PbI_2 film decreases. However, the transparent films obtained from the vacuum assistant method still ensure that all the AVT values of the TPVs are greater than 60% (Table 1) with no measurable haze. The high transparency properties of *undoped* lead halide TPVs are also partially attributed to the ultrathin lead halide films, whereas the doped lead halides can maintain higher transparency for larger thickness ranges due to bandgaps closer to the 2.7−2.8 eV cutoff. For the various lead halide films with the same precursor concentration, the transmission spectra are close to each other, especially for the transmission spectra of TPV devices (Figure S11). For example, all of the transmission spectra of 0.2 M films are higher than 70% in the range from 515 to 900 nm, and the transmission spectra of TPV devices exhibit a peak at 520 nm where the transmission exceeds 70%, resulting in AVTs around 68% for 0.2 M.

To investigate the optical properties, the reflection spectra of lead halide TPVs are further measured. The $PbI_{1.8}Br_{0.2}$ TPV device is used as a representative device to illustrate the optical properties of doped lead halide TPVs. Figure 4a shows the photograph of a complete $PbI_{1.8}Br_{0.2}$ TPV device taken under outdoor conditions. The lack of strong coloring is reflected by the high CRI value (>90). Generally, a CRI value of 90 is the lower limit for acceptable color alteration to maintain a "natural color".[1] Figure S12b shows the transmission spectra of $PbI_{1.8}Br_{0.2}$ TPVs, where the drop in transmission between 510

DOI: 10.1021/acsaem.9b00270
ACS Appl. Energy Mater. 2019, 2, 3972−3978

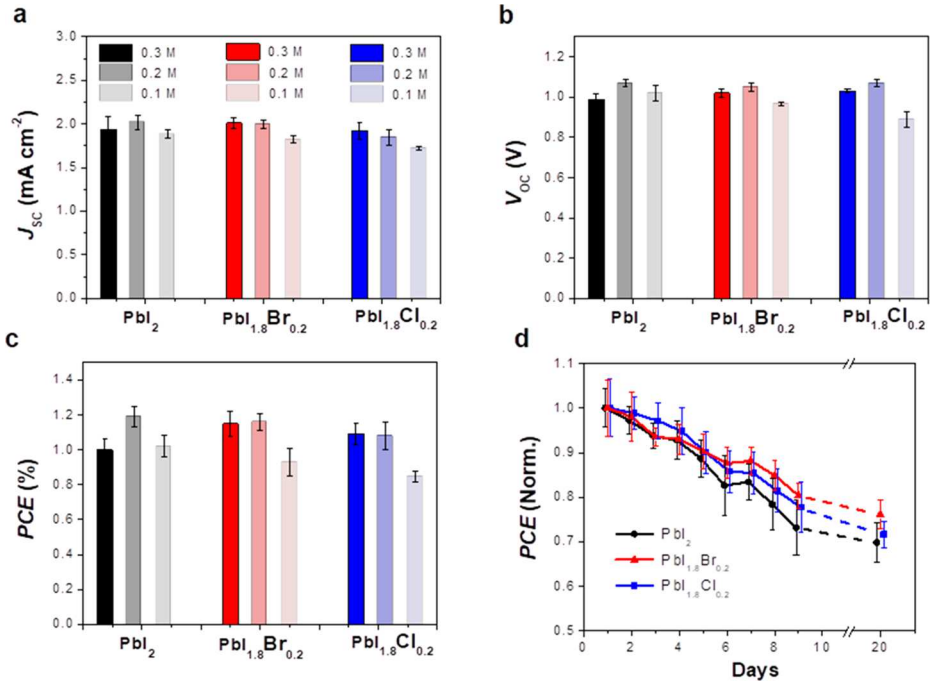

Figure 5. Parameters of various lead halide TPV devices: (a) J_{SC}, (b) V_{OC}, and (c) PCE. Parameters of PbI_2 TPVs, $PbI_{1.8}Br_{0.2}$ TPVs, and $PbI_{1.8}Cl_{0.2}$ TPVs are shown by black, red, and blue columns with various transparencies for the different concentrations, respectively. The error bars show the standard deviation for TPV devices, where two batches of devices (7−8 devices for each condition) are used for the standard deviation calculation. (d) Initial device stability measurement of lead halide TPVs.

and 900 nm compared to that of neat films is mainly caused by reflection of the top electrode (Figure 4b). With the addition of one AR coating applied on the glass side, the AVT of $PbI_{1.8}Br_{0.2}$ TPV increases from 67.5% to 69.1%. The AVTs of 0.1 M-PbI_2 and 0.1 M-$PbI_{1.8}Cl_{0.2}$ TPVs then exceed 70%.

The EQE of $PbI_{1.8}Br_{0.2}$ TPV device is also shown in Figure 4b to analyze the necessary consistency checks.[1] The devices show a maximum EQE up to 35% at 410 nm, so that the integrated photocurrent from the EQE spectrum is 1.78 mA cm^{-2}. Combined with a calculated spectral mismatch factor of 1.09, this integrated photocurrent agrees well with the short-circuit current density (J_{SC}) extracted from the J−V curve. Using the photon balance to estimate the internal quantum efficiency (IQE), the maximum IQE is calculated to be 70.1% at 465 nm by estimating the total absorption using the photon balance ($A = 1 - T - R$). Using the photon balance as a consistency check, the sum of ($T + R +$ EQE) is lower than 1.0 at every wavelength so that each of these independent measurements is unlikely to be overestimated.[1]

The photovoltaic performance of lead halide TPVs as a function of doping and thickness (concentration) is also systematically studied. The photovoltaic parameters of TPVs are summarized in Table 1 and plotted in Figure 5. The results indicate that the TPV devices have good reproducibility, and a majority of devices have PCE over 1%. Figure S5 shows the comparisons of parameters for both opaque devices and transparent devices. The opaque Ag electrode can reflect incident light and results in higher total absorption due to the "double-pass effect". With such an effect, the opaque PV can harvest a larger amount of incident photons compared to the TPVs with same PbI_2 active layer thickness. Therefore, the photocurrent densities (J_{SC}'s) of opaque PVs are all higher than those of the TPV devices, which also leads to a modestly higher PCE of the opaque PVs over TPVs. Overall, lead halide TPVs are improved in both device efficiency and transparency with PCE up to 1.22% and an AVT above 70%. To the best of our knowledge, this result is the first report for a TPV with both an AVT over 70% and a PCE over 1%. Moreover, by managing both absorption and reflection, the resulting CRI of the device is higher than the CRI of the film alone so that the device also has a more neutral, albeit slightly greenish, color.

AVT is a critically important metric, but CRI (aesthetics) is often just as important in determining whether a TPV will be viable in an application. Thus, blue-shifting the absorption edge outside of the visible spectrum is still a practical strategy to maximize PCE and CRI at the highest AVT levels, even though we have only shown modest increases in these materials. However, another important benefit of this doping is its impact on lifetime where we demonstrate the potential for increasing device stability with Br/Cl doping. The performance stability of unencapsulated TPVs is also evaluated (Figure 5d). All the devices tested can maintain efficiencies over 80% of the initial efficiency after 150 h and over 60% after 500 h. Among the TPVs studied, the $PbI_{1.8}Br_{0.2}$ device shows enhanced stability. This is similar to the results seen with halide perovskites where Br doping and analogues typically tend to be more stable (particularly in air) over purely iodide based compositions.[30] We presume that the improvement of film crystallization also contributes to the stability of the Br doped TPV device (Figure S9c). Looking ahead, it is likely that good encapsulation methods will further enhance device lifetimes well beyond these initial unencapsulated measurements.

In summary, we have developed a series of lead halide TPV devices with both high efficiency and transparency. The thickness of the lead halide layer is systematically optimized, and the bandgap and absorption of lead halide films are also tuned by doping chlorine and bromine into the pure PbI_2. While the doping range is limited by sharp device performance

DOI: 10.1021/acsaem.9b00270
ACS Appl. Energy Mater. 2019, 2, 3972−3978

reduction beyond 10% for Cl doping and 30% for Br doping, this work demonstrates that bandgap tunability is achievable, albeit with a more complex mechanism, in these materials. After device optimization the lead halide TPVs are shown to achieve a PCE over 1.0% while the AVT exceeds 70% and the CRI exceeds 90. This work reports one of the highest device efficiencies reported with the highest transparency, which provides an encouraging path to higher performance TPVs and multijunction TPVs.

EXPERIMENTAL SECTION

Materials and Precursor Preparation. Dimethylformamide (DMF, anhydrous, 99.8%, Aldrich), PbI_2 (99%, Aldrich), $PbBr_2$ (99%, Aldrich), $PbCl_2$ (98%, Aldrich), C_{60} (99.9%, MER Corporation), 2,9-dimethyl-4,7-diphenyl-1,10-phenanthroline (BCP, Lumtech), and tris(8-hydroxy-quinolinato)aluminum (Alq_3, 99.5%, Lumtech) were used as received. Poly(3,4-ethylenedioxythiophene) polystyrene sulfonate (PEDOT, Clevios PVP AI 4083, 1.3 wt %, Heraeus) was diluted to 10 vol % with deionized water before use.

To prepare the 1.0 M PbI_2 precursor solution, a 461 mg portion of PbI_2 was added to 1.0 mL DMF. The solutions were then stirred for 1 h and filtered with 0.45 μm PTFE filters. The various concentrations of PbI_2 solutions were prepared by diluting the 1 M PbI_2 solutions with DMF.

Device Fabrication. PEDOT solutions were spin-coated onto precleaned ITO substrates at 6000 rpm for 10 s and then annealed at 110 °C for 2 min. The lead halide precursor solution was spin-coated on top of the PEDOT film at 6000 rpm for 7 s; it was then moved quickly into a homemade vacuum chamber, which was evacuated to the mtorr range, and left in the chamber for 3 min. The substrates were then transferred to the hot plate and annealed at 80 °C for 2 min. The substrates were then moved into the evaporation chamber for deposition of C_{60} (20 nm) and BCP (7.5 nm). Finally, a 5 nm thick silver electrode and 60 nm of Alq_3 were deposited by thermally evaporated at a base pressure of 3×10^{-6} Torr through a shadow mask with a final measured device area of 4.85 mm^2. For the opaque device, an 80 nm silver layer was thermally deposited on the BCP layer as the electrode.

Measurement and Characterization. The thickness of the PbI_2 film was measured by spectroscopic ellipsometry (Wollam Vase). UV−vis−NIR transmission and reflection spectra were collected using a dual beam PerkinElmer Lambda 800 spectrometer. The transmission spectra are measured from the whole device including the substrate and the PV device, and no reference sample/substrate was utilized in the reference beam. Generally, the optical baseline between the test/reference sides of the dual beam spectrometer is first calibrated to determine the total beam intensity on each side. For the actual transmission measurement of the TPV device, no blank glass sample is used on the reference side (just air). The reference channel of a dual beam spectrometer is generally used to offset the reflections from a sample container (such as the quartz cuvette). However, this subtraction cannot be done so easily for thin films due to optical interference differences. The current density−voltage characteristics ($J-V$ curves) were obtained using a Keithley 2420 source measurement unit under both dark and AM1.5G solar simulation where the light intensity was measured using an NREL-calibrated Si reference cell with KG5 filter (xenon arc lamp with the spectral-mismatch factor of 1.08 ± 0.02 for the devices studied). Devices were scanned at a rate of 50 mV/s. EQE measurements were performed using a QTH lamp with a calibrated Si detector, monochromator, chopper, and lock-in amplifier. The IQE was estimated as $IQE = EQE/(1 - R - T)$. The $J-V$ and EQE were measured on unencapsulated devices/samples in ambient air. The stability test was conducted on devices without encapsulation. The devices were stored in the dark in ambient air and tested under the AM 1.5G 100 mW cm^{-2} irradiation at room temperature with a relative humidity of 16−40%.

ASSOCIATED CONTENT

Supporting Information

The Supporting Information is available free of charge on the ACS Publications website at DOI: 10.1021/acsaem.9b00270.

PbI_2 thickness measurements, SEM images of PbI_2 films, parameter statistics of opaque lead halide solar cells prepared by doped lead halide precursor solutions, and detailed transmission spectra of lead halide films and TPVs (PDF)

AUTHOR INFORMATION

Corresponding Author

*E-mail: rlunt@msu.edu.

ORCID

Richard R. Lunt: 0000-0003-4248-6312

Author Contributions

‖The authors D. L. and C.Y. made equal contribution to the work.

Notes

The authors declare the following competing financial interest(s): D.L. and R.R.L. have filed a patent application based on the work in this manuscript. R.R.L. is a co-founder, advisor, and a minority owner of Ubiquitous Energy, Inc., a company working to commercialize TPV technologies. All other authors declare no competing financial interest.

ACKNOWLEDGMENTS

The authors acknowledge financial support from the Michigan State University Strategic Partnership Grant (SPG) and from the National Science Foundation Division of Materials Research (DMR) Solid State and Materials Chemistry (SSMC) program (Award #1807573).

REFERENCES

(1) Traverse, C. J.; Pandey, R.; Barr, M. C.; Lunt, R. R. Emergence of Highly Transparent Photovoltaics for Distributed Applications. *Nat. Energy* **2017**, *2*, 849−860.

(2) Barile, C. J.; Slotcavage, D. J.; Hou, J.; Strand, M. T.; Hernandez, T. S.; McGehee, M. D. Dynamic Windows with Neutral Color, High Contrast, and Excellent Durability Using Reversible Metal Electrodeposition. *Joule* **2017**, *1*, 133−145.

(3) Li, Y.; Lin, J.-D.; Che, X.; Qu, Y.; Liu, F.; Liao, L.-S.; Forrest, S. R. High Efficiency Near-Infrared and Semitransparent Non-Fullerene Acceptor Organic Photovoltaic Cells. *J. Am. Chem. Soc.* **2017**, *139*, 17114−17119.

(4) Suddard-Bangsund, J.; Traverse, C. J.; Young, M.; Patrick, T. J.; Zhao, Y.; Lunt, R. R. Organic Salts as a Route to Energy Level Control in Low Bandgap, High Open-Circuit Voltage Organic and Transparent Solar Cells that Approach the Excitonic Voltage Limit. *Adv. Energy Mater.* **2016**, *6*, 1501659.

(5) Chen, C.-C.; Dou, L.; Zhu, R.; Chung, C.-H.; Song, T.-B.; Zheng, Y. B.; Hawks, S.; Li, G.; Weiss, P. S.; Yang, Y. Visibly Transparent Polymer Solar Cells Produced by Solution Processing. *ACS Nano* **2012**, *6*, 7185−7190.

(6) Véron, A. C.; Zhang, H.; Linden, A.; Nüesch, F.; Heier, J.; Hany, R.; Geiger, T. NIR-Absorbing Heptamethine Dyes with Tailor-Made Counterions for Application in Light to Energy Conversion. *Org. Lett.* **2014**, *16*, 1044−1047.

(7) Davy, N. C.; Sezen-Edmonds, M.; Gao, J.; Lin, X.; Liu, A.; Yao, N.; Kahn, A.; Loo, Y.-L. Pairing of Near-Ultraviolet Solar Cells with Electrochromic Windows for Smart Management of the Solar Spectrum. *Nat. Energy* **2017**, *2*, 17104.

DOI: 10.1021/acsaem.9b00270
ACS Appl. Energy Mater. 2019, 2, 3972−3978

(8) Liu, D.; Yang, C.; Lunt, R. R. Halide Perovskites for Selective Ultraviolet-Harvesting Transparent Photovoltaics. *Joule* **2018**, *2*, 1827−1837.
(9) Kwon, H.-C.; Kim, A.; Lee, H.; Lee, D.; Jeong, S.; Moon, J. Parallelized Nanopillar Perovskites for Semitransparent Solar Cells Using an Anodized Aluminum Oxide Scaffold. *Adv. Energy Mater.* **2016**, *6*, 1601055.
(10) Cao, D. H.; Stoumpos, C. C.; Malliakas, C. D.; Katz, M. J.; Farha, O. K.; Hupp, J. T.; Kanatzidis, M. G. Remnant PbI2, an unforeseen necessity in high-efficiency hybrid perovskite-based solar cells? *APL Mater.* **2014**, *2*, 091101.
(11) Renaud, A.; Grasset, F.; Dierre, B.; Uchikoshi, T.; Ohashi, N.; Takei, T.; Planchat, A.; Cario, L.; Jobic, S.; Odobel, F.; Cordier, S. Inorganic Molybdenum Clusters as Light-Harvester in All Inorganic Solar Cells: A Proof of Concept. *ChemistrySelect* **2016**, *1*, 2284−2289.
(12) Kuttipillai, P. S.; Yang, C.; Chen, P.; Wang, L.; Bates, M.; Lunt, S. Y.; Lunt, R. R. Enhanced Electroluminescence Efficiency in Metal Halide Nanocluster Based Light Emitting Diodes through Apical Halide Exchange. *ACS Applied Energy Materials* **2018**, *1*, 3587−3592.
(13) Zhao, Y.; Lunt, R. R. Transparent Luminescent Solar Concentrators for Large-Area Solar Windows Enabled by Massive Stokes-Shift Nanocluster Phosphors. *Adv. Energy Mater.* **2013**, *3*, 1143−1148.
(14) Hamdeh, U. H.; Nelson, R. D.; Ryan, B. J.; Bhattacharjee, U.; Petrich, J. W.; Panthani, M. G. Solution-Processed BiI3 Thin Films for Photovoltaic Applications: Improved Carrier Collection via Solvent Annealing. *Chem. Mater.* **2016**, *28*, 6567−6574.
(15) Dunlap-Shohl, W. A.; Hill, I. G.; Yan, Y.; Mitzi, D. B. Photovoltaic Effect in Indium(I) Iodide Thin Films. *Chem. Mater.* **2018**, *30*, 8226−8232.
(16) Tiwari, D.; Alibhai, D.; Fermin, D. J. Above 600 mV Open-Circuit Voltage BiI3 Solar Cells. *ACS Energy Lett.* **2018**, *3*, 1882−1886.
(17) Boopathi, K. M.; Hanmandlu, C.; Singh, A.; Chen, Y.-F.; Lai, C. S.; Chu, C. W. UV- and NIR-Protective Semitransparent Smart Windows Based on Metal Halide Solar Cells. *ACS Applied Energy Materials* **2018**, *1*, 632−637.
(18) Liu, D.; Gangishetty, M. K.; Kelly, T. L. Effect of CH3NH3PbI3 Thickness on Device Efficiency in Planar Heterojunction Perovskite Solar Cells. *J. Mater. Chem. A* **2014**, *2*, 19873−19881.
(19) Liu, D.; Kelly, T. L. Perovskite Solar Cells with A Planar Heterojunction Structure Prepared Using Room-Temperature Solution Processing Techniques. *Nat. Photonics* **2014**, *8*, 133−138.
(20) Burschka, J.; Pellet, N.; Moon, S.-J.; Humphry-Baker, R.; Gao, P.; Nazeeruddin, M. K.; Gratzel, M. Sequential Deposition as A Route to High-Performance Perovskite-Sensitized Solar Cells. *Nature* **2013**, *499*, 316−319.
(21) Liu, T.; Hu, Q.; Wu, J.; Chen, K.; Zhao, L.; Liu, F.; Wang, C.; Lu, H.; Jia, S.; Russell, T.; Zhu, R.; Gong, Q. Mesoporous PbI2 Scaffold for High-Performance Planar Heterojunction Perovskite Solar Cells. *Adv. Energy Mater.* **2016**, *6*, 1501890.
(22) Liu, D.; Traverse, C. J.; Chen, P.; Elinski, M.; Yang, C.; Wang, L.; Young, M.; Lunt, R. R. Aqueous-Containing Precursor Solutions for Efficient Perovskite Solar Cells. *Advanced Science* **2018**, *5*, 1700484.
(23) Brown, P. R.; Lunt, R. R.; Zhao, N.; Osedach, T. P.; Wanger, D. D.; Chang, L.-Y.; Bawendi, M. G.; Bulović, V. Improved Current Extraction from ZnO/PbS Quantum Dot Heterojunction Photovoltaics Using a MoO3 Interfacial Layer. *Nano Lett.* **2011**, *11*, 2955−2961.
(24) Li, Y.; Sun, W.; Yan, W.; Ye, S.; Peng, H.; Liu, Z.; Bian, Z.; Huang, C. High-Performance Planar Solar Cells Based On CH3NH3PbI3-xClx Perovskites with Determined Chlorine Mole Fraction. *Adv. Funct. Mater.* **2015**, *25*, 4867−4873.
(25) Zuo, C.; Ding, L. Modified PEDOT Layer Makes a 1.52 V Voc for Perovskite/PCBM Solar Cells. *Adv. Energy Mater.* **2017**, *7*, 1601193.
(26) Jiang, F.; Rong, Y.; Liu, H.; Liu, T.; Mao, L.; Meng, W.; Qin, F.; Jiang, Y.; Luo, B.; Xiong, S.; Tong, J.; Liu, Y.; Li, Z.; Han, H.; Zhou, Y. Synergistic Effect of PbI2 Passivation and Chlorine Inclusion Yielding High Open-Circuit Voltage Exceeding 1.15 V in Both Mesoscopic and Inverted Planar CH3NH3PbI3(Cl)-Based Perovskite Solar Cells. *Adv. Funct. Mater.* **2016**, *26*, 8119−8127.
(27) Stranks, S. D.; Eperon, G. E.; Grancini, G.; Menelaou, C.; Alcocer, M. J. P.; Leijtens, T.; Herz, L. M.; Petrozza, A.; Snaith, H. J. Electron-Hole Diffusion Lengths Exceeding 1 Micrometer in an Organometal Trihalide Perovskite Absorber. *Science* **2013**, *342*, 341.
(28) Jana, A.; Mittal, M.; Singla, A.; Sapra, S. Solvent-free, mechanochemical syntheses of bulk trihalide perovskites and their nanoparticles. *Chem. Commun.* **2017**, *53*, 3046−3049.
(29) Lumbreras, M.; Protas, J.; Jebbari, S.; Dirksen, G. J.; Schoonman, J. Structure and ionic conductivity of mixed lead halides PbCl2xBr2(1−x). II. *Solid State Ionics* **1986**, *20*, 295−304.
(30) Moghe, D.; Wang, L.; Traverse, C. J.; Redoute, A.; Sponseller, M.; Brown, P. R.; Bulović, V.; Lunt, R. R. All vapor-deposited lead-free doped CsSnBr3 planar solar cells. *Nano Energy* **2016**, *28*, 469−474.

DOI: 10.1021/acsaem.9b00270
ACS Appl. Energy Mater. 2019, 2, 3972−3978